Transport of 29 cm^{-1} phonons in hydrogenated amorphous silicon

A. J. Scholten, A. V. Akimov,* and J. I. Dijkhuis
Faculty of Physics and Astronomy, and Debye Institute, University of Utrecht, P.O. Box 80.000, 3508 TA Utrecht, The Netherlands
(Received 10 June 1996)

The scattering of 29 cm^{-1} phonons in hydrogenated amorphous silicon (*a*-Si:H) at 2 K is investigated by means of optically generated heat pulses and the ruby phonon detector. The transport is shown to be governed by elastic spatial diffusion and a diffusion coefficient of ~1 cm^2/s. Resonant scattering by soft oscillators, as well as Rayleigh scattering by microvoids or by the disordered network itself account for the experimental findings. In optically excited *a*-Si:H, the transmission of 29 cm^{-1} phonons is reduced by *in*elastic scattering, proportional to the optical excitation density in *a*-Si:H and recovers on a 40-ns time scale. These results are discussed in terms of interaction of 29 cm^{-1} phonons with optically generated long-lived very high-frequency phonons in *a*-Si:H. [S0163-1829(96)00541-3]

I. INTRODUCTION

It is well known that in amorphous materials phonons in the terahertz (THz) region are scattered to such a degree, that their mean free path l approaches their wavelength λ. The question of whether or not this leads to localization of the vibrational states is a controversial issue.[1] In this paper we will focus our attention on phonons that have an energy of 29 cm^{-1} (0.87 THz), and are presumably close to the Ioffe-Regel limit $l=\lambda$, as judged from the thermal conductivity data of amorphous silicon. The scattering of phonons in this frequency region is of importance in the temperature region of the heat-conductivity plateau, universally encountered in amorphous solids. Many explanations have been suggested in order to explain this remarkable plateau, for example Rayleigh scattering from either density or force-constant fluctuations,[2] that might eventually lead to phonon localization,[3,4] phonon-phonon scattering,[5] and scattering of phonons by soft modes.[6] In order to check the validity of these partly conflicting models, and to better understand the anomalous thermal conductivity in these materials, it is relevant to examine the transport of nonequilibrium terahertz phonons in amorphous materials. At present, the number of experimental studies in this field is, however, quite limited.[7–10]

In this paper, we study the transport of 29 cm^{-1} phonons on nanosecond time scales in *a*-Si:H held at 2 K. This paper is outlined as follows. In Sec. II, we will describe the experimental setup, and explain the characteristics of the so-called ruby phonon detector. In Sec. III, the experimental results for *a*-Si:H in the dark are presented and discussed. We demonstrate that the transport of 29 cm^{-1} phonons in *a*-Si:H is governed by elastic spatial diffusion, determine the diffusion coefficient, and discuss various elastic-scattering mechanisms. In Sec. IV, we present the measurements in optically excited *a*-Si:H. Here, the transmission coefficient of 29 cm^{-1} phonons through an optically excited region in *a*-Si:H is derived vs optical density and the emission of 29 cm^{-1} phonons out of the optically excited region in *a*-Si:H is monitored in a time-resolved fashion. These results are shown to be in accordance with the long decay times for high-frequency phonons, observed earlier in this material.[1] In Sec. V we summarize and conclude.

II. EXPERIMENTAL DETAILS

A. Samples

Hydrogenated amorphous silicon was deposited on sapphire (Al_2O_3) substrates by means of plasma-enhanced chemical vapor deposition. The substrates contain approximately 20-at. ppm Cr^{3+} ions, as determined from optical absorption measurements.

We used several samples in the experiments. The first sample, sample no. 1, has an *a*-Si:H layer of 700-nm thickness, deposited at 110 °C. The hydrogen concentration amounts to 19 at. %, as inferred from infrared absorption spectroscopy. The other samples have film thicknesses of 100, 250, and 700 nm, respectively, and were all deposited at 180 °C. Here, the hydrogen concentration amounts to ~10 at. %. On all samples, a 30-nm gold film was deposited that covered part of the *a*-Si:H layer and part of the bare substrate.

In order to remove thermal phonons, all experiments were carried out on a sample at 2 K, located in an immersion liquid-helium cryostat with optical access.

B. Phonon generation

Broadband heat pulses were injected either by picosecond illumination of the *a*-Si:H or, alternatively, of the gold film. Following optical excitation, namely, phonons are generated as a result of rapid carrier relaxation.[11,12] Even at the lowest excitation densities used, a helium gas bubble develops near the phonon source,[13] preventing the escape of phonons from the pumped zone directly into the liquid helium.

C. Ruby detector

The Cr^{3+} ions present in the Al_2O_3 substrates are used to detect the 29-cm^{-1} phonons arriving as part of the heat pulse from the *a*-Si:H. The heat-pulse technique was used earlier in a study of phonon transmission through amorphous germanium films.[8] The principle of the ruby detector[14] is explained using the picture in Fig. 1. Following optical excitation in the $^4T_2$ band (not shown here) and fast nonradiative

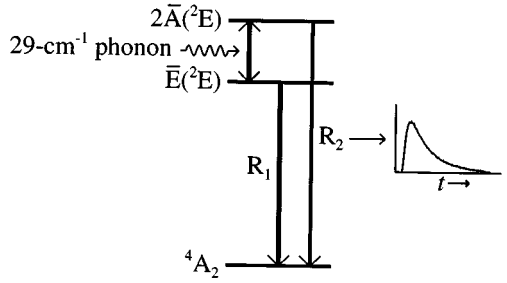

FIG. 1. Principle of the detection of 29 cm^{-1} phonons in ruby. The graph shows an example of a time-resolved R_2 luminescence measurement.

decay, the ^2E levels are populated on a picosecond time scale. At low temperatures, the upper $2A(^2E)$ level quickly decays in a direct process to the $E(^2E)$ level, under the emission of a 29 cm^{-1} phonon. The $E(^2E)$ state is metastable and decays radiatively to the $^4A_2$ ground state in 4 ms, producing the intense R_1 luminescence line. At low temperatures the lower $E(^2E)$ level is of course much higher populated than the upper $2A(^2E)$ level. Consequently, the intensity of the R_2 luminescence [transition $2A(^2E)\rightarrow{}^4A_2$] is negligible at 2 K. However, as soon as a phonon pulse appears in the optically pumped region of the crystal, the 29 cm^{-1} phonons induce a transition $E(^2E)\rightarrow 2A(^2E)$ (Fig. 1) and an R_2 luminescence pulse emerges, with an intensity proportional to the phonon occupation number, N. In equilibrium, the ratio of luminescence intensities R_2/R_1 is given by

$$\frac{R_2}{R_1}=\frac{N}{N+1}, \tag{1}$$

for small values of N reducing to $R_2/R_1=N$. Here, the radiative decay probability of $E(^2E)$ and $2A(^2E)$ are taken equal, and N is the occupation number of 29 cm^{-1} phonons on speaking terms with the $E(^2E)\rightarrow 2A(^2E)$ transition in the crystal. In absence of phonon bottlenecking,[15] i.e., for vanishing concentration of Cr^{3+} ions in $E(^2E)$, the time resolution of this detector is ultimately limited by the spontaneous phonon emission time, which amounts to 700 ps.[16]

D. Characteristics of the ruby detector

At this point, we discuss some of the properties of the ruby detector that are relevant for the interpretation and analysis of the experiments.

Phonon polarization. In our experiment, the phonon-induced R_2 luminescence is dominated by transversely polarized phonons. This is due to the fact that the density of states for longitudinal phonons is a factor $2(v_t/v_l)^3\approx 10$ lower than that of transverse phonons, both in a-Si:H and ruby. In addition, the matrix element of the coupling between $E(^2E)$ and $2A(^2E)$ is generally weaker for longitudinal phonons than for transverse.

Ballistic transport and time resolution. The nature of the transport of 29 cm^{-1} phonons in our sapphire substrates crucially determines the time resolution.[14] Multiple capture and reemission of 29 cm^{-1} phonons by the excited Cr^{3+} ions, namely, may cause diffusive, instead of ballistic transport, resulting in a so-called phonon bottleneck,[15] and adversely affect the characteristics of the detector.

In order to estimate the mean free path of 29 cm^{-1} phonons in our detector, we make a comparison with early work done in our group.[17] For excitation densities comparable with ours, a mean free path of 20 μm was found for transverse phonons in a 700-at ppm ruby crystal. Our nominally undoped samples, however, contain only approximately 20-at ppm Cr^{3+} ions, leading by linear extrapolation to a mean free path of $\sim$700 μm under otherwise the same conditions. This is much more than the radius of the optically excited region (approximately 50 μm), and suggests ballistic transport in our detector. Experimentally, we have verified the absence of bottlenecking by applying magnetic fields as high as 1.5 T, and detected no change in the decay of $R_2(t)$. This proves the absence of bottlenecking.[18] We conclude that under the present conditions the transport of 29 cm^{-1} in our detector is ballistic and makes it to act as a perfect heat sink for 29 cm^{-1} phonons.

In the present experimental geometry, we can show that the time resolution of the ruby detector is limited by the velocity of sound, and not by the $2A(^2E)\rightarrow E(^2E)$ transition rate. The phonons are detected in an excited cylinder in the sapphire which has a diameter of $d\approx 100$ μm and a length of 800 μm. In case of surface phonon injection and isotropic ballistic transport of the phonon flux $\Phi(t)$, the detected signal $R_2(t)$ is given by

$$R_2(t)\propto\int\int\int\int\int \frac{\Phi(t-|\vec{r}-\vec{r}'|/v_t)}{|\vec{r}-\vec{r}'|^2}\,dx\,dy\,dz\,dx'\,dy'. \tag{2}$$

Here, the triple integral is evaluated over the volume of the excited cylinder, and the double integral over the area of the phonon source on the detector surface ($x=0$). From numerical inspection of Eq. (2), it is seen that the major part of the phonon-induced R_2 luminescence signal is produced in the part of the excited cylinder between $x=0$ and $x\approx d/2$. Our time resolution is therefore limited to $\delta t\sim d/2v_t\sim 10$ ns, where $v_t=6400$ m/s is the sound velocity of TA phonons in Al_2O_3.

E. Apparatus

In Secs. III and IV we use a synchronously pumped, mode-locked Rhodamine 560 dye laser, equipped with a cavity dumper. We adjusted the wavelength of the laser light to match the $^4T_2$ absorption band in Al_2O_3:Cr^{3+}, $\lambda=567$ nm. The penetration depth a into the a-Si:H then is 330 nm, as checked by optical transmission experiments. The repetition rate of the cavity dumper was set to 4 MHz. The duration of the laser pulses was $\sim$25 ps, as determined by an autocorrelator.

In addition we used in Sec. IV a cavity-dumped, mode-locked Ar^+ laser, which produced light of a shorter wavelength ($\lambda=514$ nm), and smaller penetration depth (143 nm) in a-Si:H. The pulse length was 500 ps, short enough for our purposes.

The luminescence photons are collected from the substrate, imaged on the entrance slit of a double spectrometer (spectral slit width 5 cm^{-1}), and converted to electrical pulses by means of a fast Peltier-cooled photomultiplier. By

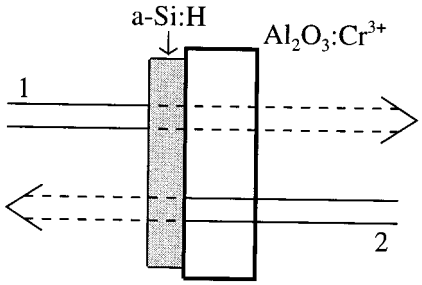

FIG. 2. Schematic picture of the experimental configurations.

means of two constant-fraction discriminators, a time-to-amplitude converter, and a pulse-height-analyzer, photons were counted with a time resolution better than 1 ns.

III. ELASTIC SCATTERING OF 29 cm^{-1} PHONONS IN COLD *a*-Si:H

A. Results

We will present the experimental results below. We include (i) experiments where phonon generation occurs in the *a*-Si:H film itself, and (ii) experiments where the gold film evaporated onto the *a*-Si:H acts as a phonon source.

(i) *Experiments with phonon excitation in a-Si:H.* Two experimental configurations are compared, schematically depicted in Fig. 2. In the first, labeled ''1,'' phonon excitation takes place from the liquid-helium side of the sample, and the detector is excited by what is left of the laser light after transmission through the *a*-Si:H layer. In the second, labeled ''2,'' the light penetrates from the sapphire side of the *a*-Si:H film. In both experiments, we use sample no. 1. The average distance that a phonon has to travel is 465 nm for configuration 1, and 235 nm for configuration 2, a difference of a factor of 2. The result of the experiment is shown in Fig. 3. Here, the R_2 luminescence intensity, divided by the corresponding R_1 luminescence intensity, is shown vs time for

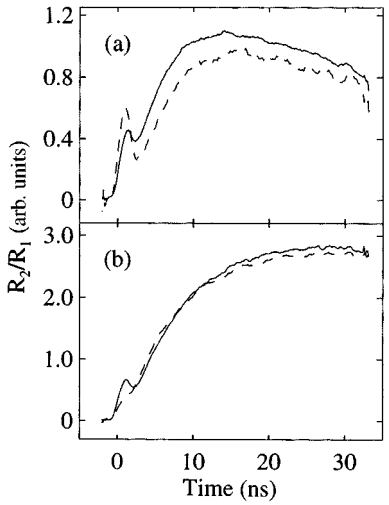

FIG. 3. Phonon signals as a function of time for two excitation densities 0.5 and 3.5 MW/m^2, for (a) and (b) respectively. The solid lines are measured in configuration 2, the dashed lines in configuration 1 (see Fig. 2).

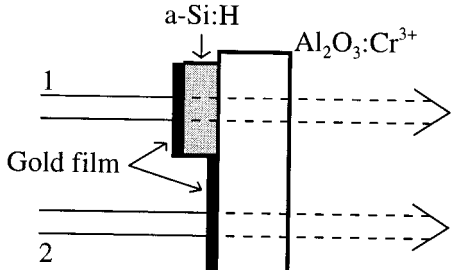

FIG. 4. Schematic picture of the experimental configurations.

configuration 1 (dotted lines) and 2 (dashed lines) for an excitation intensity of 0.5 and 3.5 MW/m^2 for Figs. 3(a) and 3(b), respectively. In both cases, we observe that the signal, according to Eq. (1) the phonon occupation number in the sapphire substrate, is virtually not affected when the phonons have to traverse a longer path through the *a*-Si:H before entering the detector. An identical result was obtained for other excitation intensities between 0.5 and 3.5 MW/m^2.

We note that the fast peaks around $t=0$ are nonresonant, not related to our detector, and probably point to surface contamination of the samples.[19] They, however, fix $t=0$ and yield the experimental time resolution of the photon counting system. For the rest, they are irrelevant to our experiments and further ignored.

(ii) *Experiments with gold-film heater.* Here, phonons are excited by illuminating the gold film on top of the *a*-Si:H film. Again, we compare two experimental configurations, schematically drawn in Fig. 4. In the first, the phonons are generated in the gold film, travel through an *a*-Si:H layer of thickness L, and enter the sapphire substrate. In the second, phonons are directly injected from the gold film into the sapphire crystal. In these experiments we have used the three 10 at. % *a*-Si:H films. The excitation density is 2.0 MW/m^2 for all curves shown.

We present the results in two different ways. First, the raw data are shown of $R_2(t)$ signals, divided by the corresponding R_1 intensities (see Fig. 5). For all films, the intensity of the phonon signal in the first configuration (solid lines) is approximately two times smaller than the signals in the second configuration (dashed curves). Apparently, phonons suffer losses in *a*-Si:H that are *independent* of the film thickness, a precursor of the phenomenon that we will discuss in Sec. IV.

Second, we normalize the curves to a common maximum intensity of 1, and examine the time dependence of the curves in more detail (see Fig. 6). It appears that the maximum of the curves is shifted a few nanoseconds when an *a*-Si:H film is present between the gold film and the substrate. This shift is most pronounced for the thickest film but hardly discernible for the 100-nm film. In sample no. 1, containing more hydrogen (19 at. %) the same results were obtained (Fig. 7).

B. Discussion

Elastic diffusion of 29 cm^{-1} phonons in cold a-Si:H. In the experiments (i), we compared two configurations with an average phonon-travel distance from generator to detector of 465 and 235 nm, respectively. In the first configuration, the

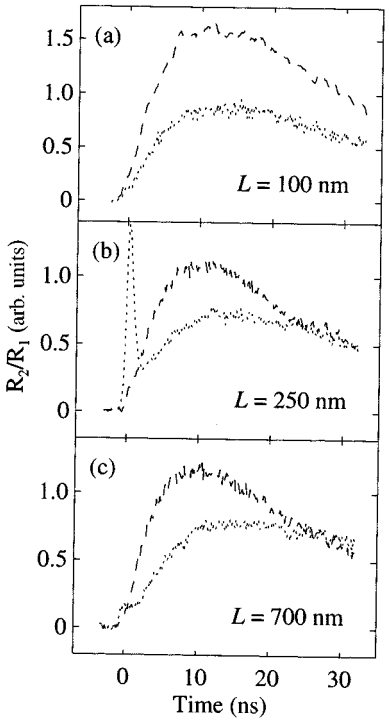

FIG. 5. Results of the experiments with a gold-film heater. Dotted curves are the time-resolved phonon signals in configuration 1, dashed curves correspond to configuration 2 (see Fig. 4).

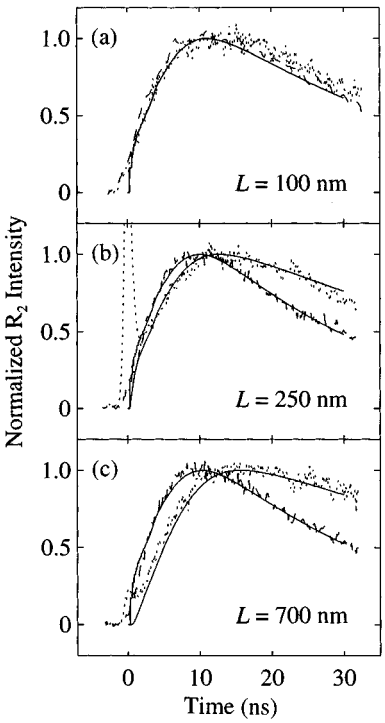

FIG. 6. The same measurements as in Fig. 5. The curves have now been normalized in order to single out the different time dependences for the two configurations of Fig. 4. Solid lines are fits, based on a simple elastic diffusion model, discussed in the text.

phonons thus have to traverse a longer path through cold a-Si:H, i.e., the part that is negligibly excited by the laser. Quite surprisingly, we can detect no loss of the phonon signal, for all excitation densities used. This directly shows that the mean free path against inelastic scattering in cold unexcited a-Si:H is much larger than $\sim$200 nm. In Sec. IV, however, we will show that inelastic processes are induced by strong optical excitation of a-Si:H. Thus our claim of the predominance of elastic scattering in a-Si:H only holds for cold a-Si:H in the dark, i.e., in the absence of significant optical excitation.

In the experiments (ii) the phonons are created in a thin gold film, injected in the a-Si:H, and travel through a-Si:H layers of thicknesses 100, 250, and 700 nm, respectively, before entering the detector. For the 100-nm film in Fig. 4(a) we observe that the phonon signal (dotted curve) has dropped by a factor of $\sim$2 with respect to the reference curve, taken with the gold film only (dashed curve), indicative for *in*elastic-scattering processes in optically excited a-Si:H (see Sec. IV). For film thicknesses greater than the penetration depth [see Figs. 5(b) and 5(c)], the phonon signals (dotted curves) remain constant, again with respect to the reference curves (dashed lines), confirming that inelastic scattering is negligible in cold a-Si:H in the dark.

Our conclusion that the scattering of 29 cm^{-1} phonons in a-Si:H is predominantly elastic is at variance with Ref. 9. Based on tunnel-junction phonon transport measurements, the authors claim to have found *in*elastic phonon scattering in a-Si:H, in a temperature and frequency range comparable to our measurement, and attribute this to atomically bonded hydrogen. They estimated the *in*elastic mean free path for $[H]=10\%$ a-Si:H to be 90–120 nm, remarkably close to what we find for the *elastic* mean free path, as we will show below. This discrepancy can be removed considering their scheme of detection around 0.875 THz, which is based on a phonon absorption resonance of interstitial oxygen in crystalline silicon. This absorption namely must depend on phonon polarization. The mean free path should then be identified with elastic TA-LA scattering, and brought into accordance with our measurements. In order to check the above suggestions, it would be interesting if the authors of Ref. 9 would repeat their measurements on a-Si:H films that are much thicker than the mean free path that they found. Finally, we note that inelastic scattering in 1-μm a-Si films was also observed in Ref. 8, but for phonons with higher frequencies ($>$0.9 THz) than in our experiments.

Diffusion coefficient. Below we treat the transport through thin cold a-Si:H samples as *elastic diffusion.* In the curves of Fig. 6, a nanosecond delay is observed as soon as the

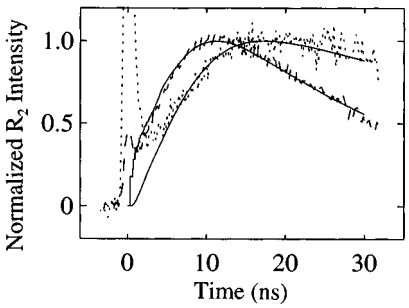

FIG. 7. Time-resolved phonon signals for sample no. 1, for an excitation density of 2.0 MW/m^2. Again, the dotted line corresponds to configuration 1, and the dashed line to configuration 2 (see Fig. 4). Solid lines are fits, discussed in the text.

phonons have to traverse an a-Si:H layer between the generator gold film and the ruby detector. The magnitude of this shift amounts to $\Delta t \sim 5$ ns for $L=700$ nm and corresponds in the case of diffusive transport to a diffusion constant of the order of $L^2/\Delta t = 1$ cm^2/s.

At this point we will present a more detailed analysis describing the shape of the measured curves, in order to extract a more precise value for the diffusion coefficient. We will neglect inelastic collisions, treat the interface with the helium as being totally reflective, and consider the sapphire substrate to be a perfect heat sink. The time resolution of the ruby detector is computed using Eq. (2). Finally, we consider transversely polarized phonons only, in both the a-Si:H and the sapphire.

The phonon injection by the gold film is approximated by an instantaneous rise followed by a simple exponential decay. To justify this, we present a numerical fit to the ''reference data'' with a gold film only, substituting the exponential decay in Eq. (2) (solid curves in Fig. 5). This calculation yields adjusted values of 25, 18, and 20 ns for the injection decay time for the $L=100$, 250, and 700 nm experiments, respectively, and a diameter of the phonon source of $d=75$ μm, a quite reasonable value.

Next we solve the diffusion equation for $n(x,t)$, the density of phonons in the a-Si:H that are resonant with the ruby detector,

$$\frac{\partial n(x,t)}{\partial t} = D \frac{\partial^2 n(x,t)}{\partial x^2} \tag{3}$$

under the condition that $n(x,0)=n_0\delta(x)$, where n_0 is the number of resonant phonons per unit area in the y-z plane, and $\delta(x)$ is the Dirac delta function, symmetric around $x=0$, consistent with total reflection of the helium interface. The solution of Eq. (3) reads

$$n(x,t) = \frac{n_0}{\sqrt{4\pi Dt}} \exp\left(-\frac{x^2}{4Dt}\right), \tag{4}$$

corresponding to a phonon flux $\phi(x,t)$, equal to

$$\phi(x,t) = -D \frac{dn(x,t)}{dx} = \frac{2\pi D n_0 x}{(4\pi Dt)^{3/2}} \exp\left(-\frac{x^2}{4Dt}\right). \tag{5}$$

Using the method of images, we further construct the boundary conditions such that the sapphire substrate acts as an ideal heat sink and let the concentration $n(L,t)$ vanish at all times. This is achieved by positioning a *negative* concentration of phonons at $x=2L$, or $n(2L,0)=-n_0\delta(x)$. To preserve symmetry around $x=0$, another negative phonon distribution has to be introduced at $x=-2L$, namely $n(-2L,0)=-n_0\delta(x)$. But by doing this we of course spoil the condition that $n(L,t)=0$ at all times. As a remedy, yet another phonon distribution is put at $x=4L$, namely $n(4L,0)=n_0\delta(x)$, and successively carrying through this procedure leads to an infinite number of image phonon distributions. This procedure yields at the a-Si:H-sapphire interface a resulting flux $\Phi(t)$, given by the following series:

$$\Phi(t) = \sum_{i=0}^{\infty} (-1)^i \frac{4\pi D n_0 (2i+1)L}{(4\pi Dt)^{3/2}} \exp\left\{-\frac{[(2i+1)L]^2}{4Dt}\right\}, \tag{6}$$

that nicely converges at any time t. We evaluate Eq. (6) numerically to a precision better than 1%. Subsequently, the calculated curves are convoluted with the exponentially decaying phonon injection, and plugged into Eq. (2) to compute $R_2(t)$.

In the fitting procedure, the cooling time of the gold film and the diffusion coefficient D are adjustable parameters. The best fits in Fig. 7 are all encountered when using $D=1.2$ cm^2/s. This value of D corresponds to a mean free path of $3D/v_t=70$ nm, making the calculation quite meaningless for the 100-nm film. The fitted decay times were 25, 38, and 45 ns for $L=100$, 250, and 700 nm, respectively. The decay time is slightly longer than found above for a gold film only, and increases for thicker a-Si:H layers, probably because the cooling of the gold film is further impeded by the amorphous layer beneath it.

The same analysis was also performed for the measurement on the film containing 19-at. % hydrogen, and yielded a value of $D=1.2$ cm^2/s and cooling times of 50 ns and 20 ns for the curves taken with and without the amorphous film, respectively.

Thus we conclude that the diffusion coefficient for 29 cm^{-1} phonons is 1.2 cm^2/s, which corresponds to a mean free path of 70 nm and an elastic-scattering time of $\tau_{\rm el}=3D/v_t^2=15$ ps. Since values here have an estimated error of 50%, differences could unfortunately not be detected between various samples. From the average time spent in the thickest a-Si:H layer, a lower limit is found for the inelastic-scattering time, $\tau_{\rm inel} \gtrsim L^2/2D=2$ ns.

C. Elastic-scattering mechanisms

We now review possible candidates that cause elastic scattering in a-Si:H: (i) soft potentials,[20] arising from, e.g., Si-H bonds, (ii) microvoids, abundantly present in a-Si:H,[21] and (iii) intrinsic disorder of the amorphous silicon network:

(i)*Soft potentials.* The soft-potential model, an extension of the well-known two-level system model, is capable of explaining the thermal properties of amorphous solids up to 100 K.[22] It postulates the existence of ''soft potentials,'' which are local defects with small harmonic constants. In case the lowest energy levels have a separation smaller than a characteristic energy W, they reduce to two-level systems. At energies $E \gg W$ one speaks of ''soft oscillators,'' which are quasilocal almost-harmonic vibrations. The energy W is typically 2–6 cm^{-1} (3–10 K), so we anticipate resonant scattering of 29 cm^{-1} phonons with soft oscillators.[23] This process is characterized by an interruption time $\tau_{\rm el}$ and generally leads to a diffusion constant,[17]

$$D = \frac{v_s^2 \tau_{\rm el}^2}{3(T_1+\tau_{\rm el})}, \tag{7}$$

with T_1 the spontaneous emission time of a soft oscillator. This equation expresses the fact that a resonant scattering event is not instantaneous, but has a duration that is, in absence of stimulated emission, equal to T_1, which is in our case related to $\tau_{\rm el}$ by

$$T_1 = \tau_{\rm el} \frac{\mathcal{D}_{\rm so}}{\mathcal{D}_{\rm ph}}. \tag{8}$$

Here, $\mathcal{D}_{so}$ and $\mathcal{D}_{ph}$ are the densities of states for soft oscillators and phonons, respectively. Using the estimate $\mathcal{D}_{so}/\mathcal{D}_{ph}\sim 2$ at $\hbar\omega=29$ cm^{-1},[24] we derive from Eq. (8) that τ_{el} must be $\sim$50 ps in order to find the experimental diffusion coefficient by means of Eq. (7).

The resonant scattering rate by soft oscillators is[23]

$$\frac{1}{\tau_{el}} \approx \frac{\pi\omega C}{6\sqrt{2}} \left(\frac{\hbar\omega}{W}\right)^3, \tag{9}$$

where C is a dimensionless parameter. Identifying the measured elastic-scattering rate $\tau_{el}=50$ ps with Eq. (9) yields

$$\frac{C}{W^3} = 5\times 10^{61}\ \text{J}^{-3}. \tag{10}$$

How realistic is this value for CW^{-3} for a-Si:H? The dimensionless parameter C normally follows from the dependence of the low-temperature sound velocity on temperature.[25] These data are not available for a-Si:H. Therefore, we adopt $C\sim 10^{-4}$, a value found in nearly all amorphous solids studied until now.[25] Then, we find $W\approx 6$ cm^{-1}, or 9 K, a quite reasonable value.

It is of interest next to find out if the absence of inelastic scattering in a-Si:H that we demonstrated above at 2 K is consistent with the predictions of the soft-potential model when we identify the scattering by soft oscillators as the main source of elastic scattering. To address this point we resort to the treatment by Kozub *et al.*[20] At low temperatures, the relevant inelastic processes are (1) nonresonant absorption of a phonon with frequency ω by a soft oscillator with energy $E<\hbar\omega$, accompanied by the emission of a phonon taking up the difference in energy, (2) resonant absorption of a phonon by a soft oscillator, followed by the emission of two phonons of lower energy. The rates of both processes turn out to be comparable in magnitude. Acting together, they yield an inelastic-scattering rate at low temperatures $T\ll W/k_B$

$$\frac{1}{\tau_{inel}} \approx \frac{4\sqrt{2}}{27\pi} \left(\frac{\Lambda\,\eta_L^2}{W}\right)^2 \omega\sqrt{\eta_L} C\left(\frac{\hbar\omega}{W}\right). \tag{11}$$

Here, Λ is the so-called bilinear coupling constant, which is of the order of the atomic energy, $\sim$10 eV. The dimensionless parameter η_L is typically 10^{-2}. From Eqs. (9) and (11) the ratio of elastic- and inelastic-scattering times is obtained

$$\frac{\tau_{el}}{\tau_{inel}} = \frac{48}{27}\ \eta_L^{9/2}\left(\frac{\Lambda}{\hbar\omega}\right)^2. \tag{12}$$

Using the experimental lower limit for the inelastic scattering time, ($\sim$2 ns), we find a ratio smaller than 0.025. For $\eta_L\approx 10^{-2}$, we arrive at $\Lambda\lesssim 13$ eV, quite a reasonable value. Thus the experimental finding that inelastic scattering is negligible in cold a-Si:H does not exclude elastic diffusion governed by resonant scattering by soft oscillators.

(ii) *Voids*. Next, we discuss elastic phonon scattering by microvoids. Evidence for the existence of these microscopic cavities in a-Si:H is abundant from small-angle x-ray (SAXS) experiments.[21] Microvoids typically have a radius of 0.5 nm, about ten times smaller than the wavelength of 29 cm^{-1} phonons in a-Si:H and act as point scatterers. The cross section γ for transverse-phonon scattering off a spherical cavity with radius r is given by[26]

$$\gamma = \zeta(\pi r^2)(kr)^4. \tag{13}$$

The numerical factor ζ depends in a complex manner on the ratio of transverse and longitudinal sound velocities.[26] For a-Si:H, this ratio is approximately 0.6 which gives $\zeta\approx 1$. Neglecting mode conversion, the mean free path l for transverse phonons may now be calculated according to $1/l=n_{void}\gamma$.

SAXS measurements yield a concentration of the voids $n_{void}=5\times 10^{19}$ cm^{-3}, and a typical void radius $r=0.43$ nm.[21] Recalling that x rays scatter from the electrons, and phonons from the nuclei, we add the atomic radius of silicon (0.12 nm) to this value, and arrive at $r=0.55$ nm. With these values for r and n_{void}, we compute a mean free path of 160 nm for transversely polarized phonons, which exceeds the experimental result by only a factor of $\sim$2. However, because of the r^6 dependence of Eq. (13), taking into account the (unknown) *distribution* of void sizes and shapes will enhance the cross section considerably, since the average $\langle r^6\rangle$ always exceeds the average $\langle r\rangle^6$. This suggests that Rayleigh scattering is an important scattering mechanism in our experiment.

(iii) *Disorder-induced Rayleigh scattering*. In any inhomogeneous material, phonons will suffer from Rayleigh scattering if the phonon wavelength is large relative to the size of the local fluctuations in the composition.[27] Rayleigh scattering by voids, discussed above, is just a special case of disorder-induced Rayleigh scattering. Nonresonant elastic scattering by soft potentials is another special case, but may be ignored for $\hbar\omega\gg W$, being much weaker than the resonant scattering by these entities.

A contribution that we did not consider yet, operative in any amorphous solid, even in absence of soft potentials and voids, is the Rayleigh scattering by the disordered network itself. This contribution was estimated by Zaitlin and Anderson[28] on the basis of the Rayleigh-Klemens law for scattering by point imperfections in crystals.[29] Their estimate for the phonon mean free path l against Rayleigh scattering in an amorphous material is

$$\overline{l} \approx 0.2\ \text{mK}^4\left(\frac{k_B}{\hbar\omega}\right)^4, \tag{14}$$

yielding $\overline{l}=67$ nm for 29 cm^{-1} phonons, in close agreement with our experimental result of 70 nm. This agreement is perhaps fortuitous, but it forms a basis to conclude that this type of scattering has at least a significant contribution.

In conclusion, all three scattering mechanisms discussed above seem to possess cross sections that are of the right order of magnitude to explain our data. However, it is not possible to estimate the relative contribution of each, due to the uncertainty in both the experimental results and the calculations.

IV. INELASTIC SCATTERING OF 29 cm^{-1} PHONONS IN OPTICALLY EXCITED a-Si:H

A. Experimental configuration

In this experiment, we investigate the transport of 29 cm^{-1} phonons through a laser-excited region in a-Si:H.

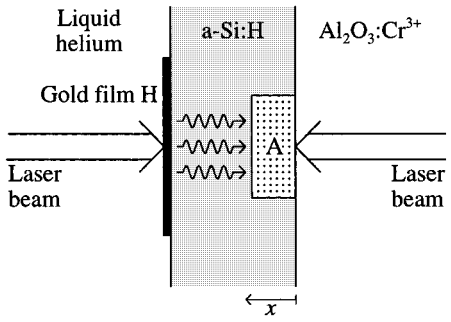

FIG. 8. Scheme of the phonon absorption experiment.

As illustrated in Fig. 8, we consider a phonon flux passing through a region A in a-Si:H, that is pumped by pulsed laser excitation. The excitation density $E_A(x)$ is defined as the absorbed pulse energy per unit volume, with x positive towards the helium surface and $x=0$ located at the interface between the a-Si:H film and the sapphire substrate. Because $E_A(x)$ decays exponentially with respect to x, the excitation density at this interface, denoted E_{0A}, is equal to the pulse energy per unit area, divided by the penetration depth a.

The initial phonon flux in the form of a heat pulse is generated by means of pulsed laser excitation of the gold film, H. The pulsed phonon injection intensity is kept constant during the experiments. After injection into a-Si:H, the heat pulse travels diffusively and traverses the excited region A, just opposite to H. The heating of H and the optical pumping of A simultaneously occurs using two beams derived from the same laser, that were focused to either side of the sample to a spot with a diameter of ~ 100 μm. Optimization of the focus and spatial overlap of the spots were achieved by means of a 100-μm pinhole, mounted on the surface of the gold film. The ruby detector is prepared by both laser beams, and used to detect the 29 cm^{-1} phonons, arriving from both H and A.

We also study the emission of 29 cm^{-1} phonons from region A in a-Si:H. This beam simultaneously creates the excited region A and prepares the sapphire phonon detector, allowing for the time-resolved probing of the emitted phonons.

B. Results

We now present the phonon absorption experiments. The gold film H is excited with a constant pulse energy per unit area of 300 mJ/mm^2. E_A can be varied both by changing the power and the penetration depth of the exciting laser light.

In each experiment, we successively measure (i) the heat-pulse-induced luminescence in absence of excitation of A, R^0_{2H}, and R_{1H}, yielding N^0_H, the corresponding phonon occupation number in the sapphire crystal; (ii) the luminescence pulse induced by phonons when exciting A only (i.e., in absence of the heat pulse from H), R^0_{2A}, and R_{1A}, yielding N^0_A, the corresponding phonon occupation number in the sapphire crystal; (iii) the luminescence signal when both A and H are excited, $R_{2(A+H)}$, and $R_{1(A+H)}$, yielding the sum of N_A and N_H (*without* superscript ''0''), the corresponding phonon occupation numbers in the sapphire crystal, effected by A and H, respectively. We note that $R_{1H} \ll R_{1A}$, due to the strong absorption of the laser light in the gold film and the a-Si:H film, and, of course $R_{1(A+H)}=R_{1A}+R_{1H}$, as checked experimentally.

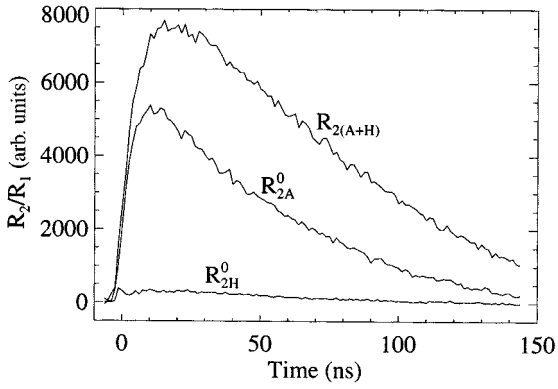

FIG. 9. Example of a set of time-resolved R_2 luminescence measurements. R^0_{2H} is measured in the absence of A, R^0_{2A} in the absence of H, and $R_{2(A+H)}$ in the presence of both A and H.

Figure 9 shows an example of a time-resolved measurement of the R^0_{2H}, R^0_{2A}, and $R_{2(A+H)}$ luminescence signals. Such sets of curves were measured for a range of excitation densities E_{0A}. In Fig. 10 we plot ΔR_2, defined as

$$\Delta R_2 \equiv R_{2(A+H)} - R^0_{2H} - R^0_{2A}\left(1+\frac{R_{1H}}{R_{1A}}\right), \qquad (15)$$

at two rather arbitrary instants of time, $t=15$ ns and $t=100$ ns, and for two laser wavelengths $\lambda=567$ nm and $\lambda=514$ nm. For $t=100$ ns a linear dependence on E_{0A} is found, while at $t=15$ ns the dependences strongly deviate from be-

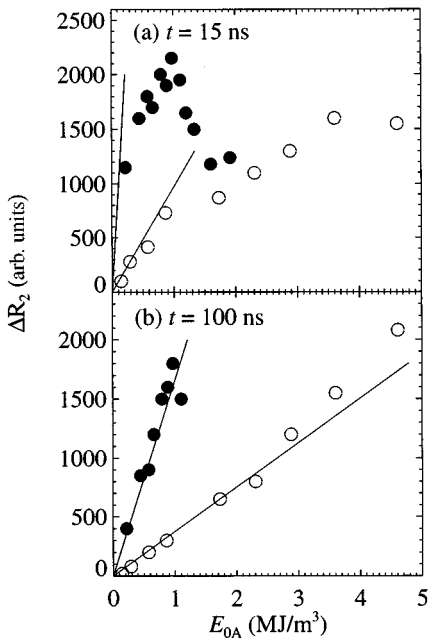

FIG. 10. ΔR_2 vs E_{0A}, measured at $t=15$ ns (a) and at $t=100$ ns (b), with $\lambda=567$ nm (●) and $\lambda=514$ nm, (○), corresponding to penetration depths of 330 and 143 nm, respectively. Straight lines show the corresponding ΔR_2, expected in the absence of phonon absorption. Deviation from the straight lines in (a) signifies phonon absorption.

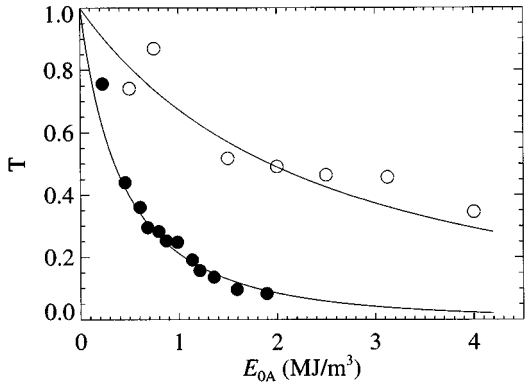

FIG. 11. Phonon transmission T vs E_{0A}, at $t=15$ ns, for $\lambda=567$ nm (●) and for $\lambda=514$ nm (○), corresponding to penetration depths of 330 and 143 nm, respectively. Solid lines are fits to the data, as explained in text.

ing linear for both excitation wavelengths. The linear dependence directly shows that no phonon absorption takes place in region A, because in that case it can be derived from Eq. (1), that $\Delta R_2 \propto R_{1A} \propto E_{0A}$. The sublinear dependence at $t=15$ ns, however, tells us that 29 cm^{-1} phonons are significantly *absorbed* at $t=15$ ns in region A.

The straight lines in the upper panel of Fig. 10 are the extrapolated values of ΔR_2 in absence of absorption, $\Delta R_2^{\text{no abs}}$, as computed by multiplying the slope of the $t=100$-ns straight line by the factor $R^0_{2H}(15\text{ ns})/R^0_{2H}(100\text{ ns})$. For the case of $\lambda=514$ nm (open circles), the straight line tracks the data points at low E_{0A}, corresponding to the absence of phonon absorption. For $\lambda=567$ nm, however, no data point touches the expected line. This implies that, already at the lowest power, absorption is present for this wavelength.

We can now straightforwardly compute the transmission coefficient $T \equiv N_H/N^0_H$

$$T \approx \frac{\Delta R_2/\Delta R_2^{\text{no abs}} + R_{1H}/R_{1A}}{1+R_{1H}/R_{1A}}. \tag{16}$$

The phonon transmission coefficient is presented in Fig. 11, where the open and solid circles refer to the penetration depths $a=143$ and 330 nm, respectively. The solid lines are fits that will be discussed in the analysis of Sec. IV C.

Finally we examine 29 cm^{-1} phonon emission from region A in a-Si:H. Figure 12 shows the $R_{2A}(t)$ luminescence signals measured for different excitation densities ($E_{0A}=0.5$–8.4 MJ/m^3) and for the two laser wavelengths. The $R_{2A}(t)$ signals exhibit two important features. First, the total duration of the R_2 pulses increases with E_{0A} and a, mainly in the form of a flattening of the top of the R^0_{2A} pulse around $t \approx 15$ ns. Second, at $t>30$ ns all the $R_{2A}(t)$ curves display an identical decay of ~45 ns, i.e., independent of both E_{0A} and a.

In Fig. 13(a) we present the dependences of the phonon signal $N_A=R_{2A}/R_{1A}$ as they were measured at $t=15$ ns vs the excitation density E_{0A}. In Fig. 13(b), the data for $t=65$ ns are shown. The solid drawn curves in Fig. 13 correspond to a 29 cm^{-1} phonon generation that is linear in E_{0A}, as will be discussed in Sec. IV C.

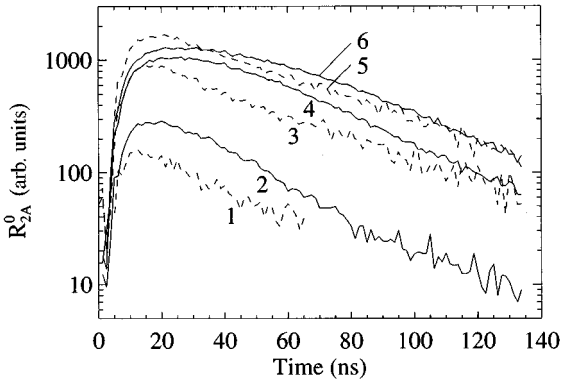

FIG. 12. Time traces of the R_2 luminescence for different excitation densities P_A and penetration depths a. The dashed curves 1, 3, and 5 are measured for $\lambda=514$ nm, with excitation intensities P_A of 0.24, 0.72, and 1.2 J/m^2, respectively. The solid curves 2, 4, and 6 are taken for $\lambda=567$ nm, with $P_A=0.18$, 0.46, and 0.62 J/m^2, respectively.

C. Analysis

From the data presented above, we wish to extract the empirical relations that catch the dependence of the absorption and generation rates of 29 cm^{-1} phonons on E_{0A}. Therefore, we consider in a phenomenological way the diffusion of 29 cm^{-1} phonons in an absorbing region A, where, additionally, 29 cm^{-1} phonons are generated according to a time- and space-dependent generation rate $G(x,t)$, that further depends on E_{0A}. The incoming phonon flux ϕ_{in} from the heater H traverses region A and can be absorbed. The outcoming flux at the a-Si:H-sapphire boundary (ϕ_{out}), in turn flows ballistically into the sapphire and is finally measured.

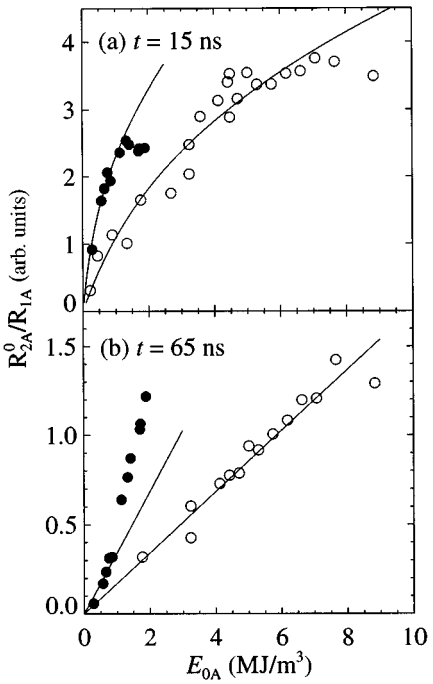

FIG. 13. The dependence of the ratio R_{2A}/R_{1A} on E_{0A}, measured at $t=15$ ns (a) and 65 ns (b) for penetration depths $a=140$ nm (○) and $a=250$ nm (●). The solid lines are based on the assumption of linear phonon generation, as explained in the text. Deviations from these curves imply nonlinear phonon generation.

The diffusion equation reads

$$D\,\frac{\partial^2 n(x,t)}{\partial x^2}-w(x,t)n(x,t)+G(x,t)-\frac{\partial n(x,t)}{\partial t}=0, \tag{17}$$

where $w(x,t)n(x,t)$ is the balance between absorption and stimulated emission of 29 cm^{-1} phonons in A. Assuming that the absorption rate $w(x,t)n(x,t)$ in Eq. (17) greatly exceeds the term $\partial n(x,t)/\partial t$, we are left with the quasistationary case

$$D\,\frac{d^2 n(x)}{dx^2}-w(x)n(x)+G(x)=0. \tag{18}$$

For reasons of tractability, we further approximate the exponentially decaying excitation density in space in the a-Si:H layer as being a constant E_{0A} for $x<a$, and zero for $x>a$, and replace $w(x)$ and $G(x)$ by a constant w and G for $x<a$, and zero for $x>a$. Solving Eq. (18) we arrive at a density of 29 cm^{-1} phonons

$$n(x)=\frac{Ga^2}{D\eta^2}\left[1+\beta_1\exp\left(\frac{\eta x}{a}\right)+\beta_2\exp\left(\frac{-\eta x}{a}\right)\right], \tag{19}$$

where β_1 and β_2 are constants to be determined from the boundary conditions, and η is given by

$$\eta=a\sqrt{\frac{w}{D}}. \tag{20}$$

The first boundary condition is that the flux $\Phi=-D[dn(x)/dx]_{x=a}$ is equal to $\phi_{\rm in}$. The second boundary condition follows from the consideration that the substrate acts as a heat sink, and forces a vanishing $n(x)$ at the a-Si:H-sapphire interface, or $[n(x)]_{x=0}=0$. Inserting these boundary conditions we arrive at a formula for the outgoing flux

$$\phi_{\rm out}=\frac{Ga}{\eta}\tanh\eta+\frac{\phi_{\rm in}}{\cosh\eta}. \tag{21}$$

This formula contains an emission term proportional to G and an absorption term proportional to $\Phi_{\rm in}$, and serves to interpret both the absorption and emission experiment.

We first analyze the absorption experiment. In the following the emission term is taken to be due only to the optical excitation of A and not affected by phonon injection from H. In fact, this emission term and other contributions to $\phi_{\rm in}$ and $\phi_{\rm out}$ caused by A, are subtracted in our transmission experiment. What we do measure is the ratio $T=\phi_{\rm out}^H/\phi_{\rm in}^H$, where $\phi_{\rm in}^H$ and $\phi_{\rm out}^H$ denote the contributions to $\phi_{\rm in}$ and $\phi_{\rm out}$ caused by the excitation of region H. According to Eq. (21), T equals

$$T=\frac{1}{\cosh\eta}. \tag{22}$$

Adopting a power-law dependence of the net absorption rate w on E_{0A}, $w(E_{0A})=(\xi E_{0A})^k$, and using Eq. (22), we adjust the parameters ξ and k such, to fit all the experimental results of Fig. 11 simultaneously using $D=1.2$ cm^2/s from Sec. III. This yields $k=1.0\pm0.2$. For $k=1$, we find $\xi=5.5\times10^3$ m^3 J^{-1} s^{-1} (the solid curves in Fig. 11). Thus, the empirical relation that we find reads

$$w(E_{0A})=\xi E_{0A}, \tag{23}$$

with $\xi=5.5\times10^3$ J m^{-3} s^{-1}. Indeed, the value $E_{0A}=10^6$ J/m^3 already leads to an absorption probability of $w\sim5\times10^9$ s^{-1}, sufficiently rapid to justify the quasistationary assumption in deriving Eq. (22).

(ii) *Emission experiment.* Next we analyze the phonon emission experiments. Here, the flux $\phi_{\rm in}$ is negative and equal to the phonon flux into the helium, and will be neglected. We substitute $\phi_{\rm in}=0$ into Eq. (21), and arrive at

$$\frac{R_{2a}^0}{R_{1a}}\propto\frac{G}{\eta}\tanh\eta, \tag{24}$$

where η is connected to w [Eq. (20)], which in turn is known as a function of E_{0A}, see Eq. (23). This enables us to single out the dependence of the generation rate G on E_{0A}.

To born this further out, let us assume for the moment a linear dependence of $G(E_{0A})$ on E_{0A}, and compare Eq. (24) with the experimental results for $t=15$ ns. For $a=330$ nm (solid circles), the data are indeed well described by a linear dependence of G on E_{0A} up to $E_{0A}\approx1.5$ M J/m^3. Above this excitation density, the data significantly drop below the solid curve, implying a strongly sublinear dependence of $G(E_{0A})$ on E_{0A} in this regime. This effect is less pronounced or possibly even absent for the $a=143$-nm data. Only the last two data points seem to indicate sublinear phonon generation.

At $t=65$ ns, the situation is markedly different. For $a=143$ nm (open circles), a linear dependence of the emitted signal on E_{0A} is observed. In this case we have $w=0$, and Eq. (24) reduces to $N_A^0\propto G_0$. Thus the linear behavior of the $a=143$-nm data not only indicates the absence of phonon absorption processes at this instant of time but also a phonon generation term that is linear in E_{0A}. For $a=330$ nm, the data show a linear rise up to $E_{0A}\approx1$ M J/m^3. For higher excitation densities a superlinear E_{0A} dependence is observed, suggesting a superlinear dependence of G on E_{0A} as well. It appears that the point where the superlinear rise sets in, almost coincides with the onset of the sublinear phonon generation at $t=15$ ns.

D. Discussion

The experimentally observed absorption of THz phonons indicates the existence of inelastic phonon scattering in optically excited a-Si:H. The inelastic scattering of 29 cm^{-1} phonons in a heat-pulse-induced ''hot spot'' was studied earlier in a crystal.[30] In these experiments, the effect of inelastic scattering was much weaker (5%) and survived much longer (2 μs) than in our a-Si:H experiments. Thus we seek a scattering mechanism that is typical for amorphous materials.

As a result of this scattering process the THz phonons should finally be converted to an excitation that may reach the temperature bath. If the absorbed energy is released in the form of phonons, we need to look for an anharmonic process which down-converts THz phonons to low-energy phonons that escape easily from the hot region by virtue of their long mean free path. In this connection we note that the

measured absorption process is characterized by a decay time of ~50 ns, which is remarkably close to the decay times (up to 70 ns) of vibrations ($150<\hbar\omega<480$ cm^{-1}), found in Ref. 1. This leads us to believe that it is the interaction of THz phonons with these long-lived high-frequency phonons that causes the experimentally observed absorption. In Ref. 1, the population of these high-frequency phonons was shown to depend linearly on excitation density, as does the absorption effect in the present experiments.

As a mechanism for the down conversion of THz phonons in *a*-Si:H at cryogenic temperatures, we suggest phonon-assisted hopping between localized high-frequency vibrations. At first sight, the large value of the inelastic-scattering rate ($w\sim5\times10^9$ s^{-1}) already at low optical pumping, seems incompatible with the slow anharmonic relaxation rate ($\sim10^7$ s^{-1}) of the high-energy vibrations observed in the experiments of Ref. 1. In an amorphous solid, this discrepancy can be remedied in a natural way by assuming a broad distribution of relaxation times, ranging from 10^{-13} up to 10^{-7} s.[31] The fast three-phonon processes, then, connect the localized vibrations nearby, cause the THz phonon absorption followed by down conversion and spatial escape of the end products, and lead to a local quasiequilibrium. The slow processes, in turn, connect the regions of quasiequilibrium, presumably located around a local minimum in vibrational frequency. These are more distant from each other and give rise to spatial transport and the slow decay of vibrational energy observed in Ref. 1. Only after the long-lived vibrations have been broken up, say after tens of nanoseconds, the THz phonon absorption disappears.

The model also explains the results of the emission experiments in terms of the decay of the high-frequency vibrations. Obviously, the generation rate of THz phonons is in this case proportional to the number of excited long-lived vibrations, and tracks the slow decay. Nonlinear effects in the phonon generation are expected when the occupation numbers of these long-lived vibrations become of the order of 1. This situation may be easily reached for moderate excitation density due to the small density of states of the long-lived vibrations and their long lifetime.

Alternatively, the THz phonons may scatter from charge carriers. It is known, however, that hot charge carriers in *a*-Si:H decay very rapidly, i.e., faster than 1 ps, to the band tail states,[11] where they are trapped for times that range from microseconds up to milliseconds.[32] Thus the relevant time scale of the dynamics of charge carriers seems incompatible with the experimental observation of an inelastic-scattering process that vanishes on a 10-ns time scale.

V. SUMMARY AND CONCLUSION

Let us summarize the main results of our experiments on 29 cm^{-1} phonons in *a*-Si:H. In Sec. III, we have demonstrated that 29 cm^{-1} phonons propagate through *a*-Si:H at 2 K by means of elastic diffusion, and extracted a diffusion coefficient of $D=1.2$ cm^2/s. It was found that resonant scattering by soft oscillators, as well as Rayleigh scattering by microvoids or by the disordered network itself are of the right order of magnitude to contribute to the measured scattering rate.

In Sec. IV, significant absorption of 29 cm^{-1} phonons was observed as soon as we optically excite *a*-Si:H. The absorption appears to depend linearly on the intensity of illumination E_{0A}. This inelastic scattering, however, is absent for longer times after firing the exciting laser pulse, say after 100 ns. In addition to this linear absorption, nonlinear effects were observed in the dependence of the phonon feeding rate on E_{0A}, becoming prominent above an energy density of ~1 M J/m^3 for a penetration depth of 330 nm. In case of a penetration depth of 143 nm, this nonlinearity was absent to at least $E_{0A}\gtrsim7$M J/m^3. Quite strikingly, a long time constant of the order of 45 ns was found in all the 29 cm^{-1} phonon emission curves, measured for different laser powers and penetration depths.

We proposed anharmonic interaction of 29 cm^{-1} phonons with localized high-frequency phonons to be responsible for the experimentally found absorption. This relates the decay times of high-frequency vibrations, measured in Ref. 1, naturally to the time scale of the disappearance of the absorption effect. Moreover, the 45-ns tail in the emission curves is explained by the assumption that the high-frequency phonon decay process is responsible for the generation of 29 cm^{-1} phonons in *a*-Si:H. The linear dependence of absorption and emission on excitation density also follows from the model. Both the experiments and the proposed model show the profound influence of the long-lived high-frequency phonon populations on the dynamics of THz phonons in optically excited *a*-Si:H.

ACKNOWLEDGMENTS

We thank F. J. M. Wollenberg and C. R. de Kok for technical assistance. We acknowledge M. Kars, J. Bezemer, and W. van Sark for providing the *a*-Si:H samples. We are grateful to the ''Nederlandse Organisatie voor Zuiver Wetenschappelijk Onderzoek (NWO)'' and INTAS (Grant No. 94-395) for financial support.

*Permanent address: A. F. Ioffe Physical-Technical Institute, 194021 St. Petersburg, Russia.

[1] A. J. Scholten, A. V. Akimov, and J. I. Dijkhuis, Phys. Rev. B **47**, 13 910 (1993); A. J. Scholten, A. V. Akimov, P. A. W. E. Verleg, J. I. Dijkhuis, and R. S. Meltzer, J. Non-Cryst. Solids **164-166**, 923 (1993); A. J. Scholten and J. I. Dijkhuis, Phys. Rev. B **53**, 3837 (1996).

[2] D. Walton, Solid State Commun. **14**, 335 (1974); D. Walton, Phys. Rev. B **16**, 3723 (1977).

[3] S. John, H. Sompolinsky, and M. J. Stephen, Phys. Rev. B **27**, 5592 (1983); T. R. Kirkpatrick, *ibid*. **31**, 5746 (1985); J. E. Graebner, B. Golding, and L. C. Allen, *ibid*. **34**, 5696 (1986).

[4] S. Alexander, C. Laermans, R. Orbach, and H. M. Rosenberg, Phys. Rev. B **28**, 4615 (1983).

[5] D. P. Jones, N. Thomas, and W. A. Phillips, Philos. Mag. B **38**, 271 (1978).

[6] V. G. Karpov and D. A. Parshin, Zh. Eksp. Teor. Fiz. 88, 2212 (1985) [Sov. Phys. JETP **61**, 1308 (1985)]; L. Gil, M. A. Ramos, A. Bringer, and U. Buchenau, Phys. Rev. Lett. **70**, 182 (1993).

[7] W. Dietsche and H. Kinder, Phys. Rev. Lett. **43**, 1413 (1979); A. S. Alekseev, M. M. Bonch-Osmolovskiĭ, T. I. Galkina, I. B. Levinson, and D. P. Utkin-Édin, Pis'ma Zh. Eksp. Teor. Fiz. **10**,

490 (1983) [JETP Lett. **37**, 582 (1983)]; U. Strom, J. C. Culbertson, P. B. Klein, and S. A. Wolf, in *Phonon Scattering in Condensed Matter*, edited by W. Eisenmenger, K. Laβman, and S. Döttinger (Springer-Verlag, Berlin, 1984), p. 338.

[8] A. V. Akimov, A. A. Kaplyanskiĭ, J. Kočka, E. S. Moskalenko, and J. Stuchlik, Zh. Eksp. Teor. Fiz. **100**, 1340 (1991) [Sov. Phys. JETP **73**, 742 (1991)]; A. A. Kaplyanskiĭ, A. V. Akimov, S. A. Basun, S. P. Feofilov, E. S. Moskalenko, J. Kočka, and J. Stuchlik, J. Lumin. **53**, 7 (1992).

[9] J. Mebert and W. Eisenmenger, Z. Phys. B **95**, 231 (1994).

[10] A. J. Scholten, A. V. Akimov, and J. I. Dijkhuis, in *22nd International Conference on the Physics of Semiconductors*, edited by D. J. Lockwood (World Scientific, Singapore, 1995), p. 2673.

[11] Z. Vardeny and J. Tauc, Phys. Rev. Lett. **46**, 1223 (1981).

[12] M. N. Wybourne and J. K. Wigmore, in *Phonon Scattering in Condensed Matter V*, edited by A. C. Anderson and J. P. Wolfe (Springer-Verlag, Berlin, 1986), p. 168.

[13] J. A. Shields, M. E. Msall, M. S. Carroll, and J. P. Wolfe, Phys. Rev. B **47**, 12 510 (1993).

[14] K. F. Renk and J. Deisenhofer, Phys. Rev. Lett. **26**, 764 (1971).

[15] J. I. Dijkhuis, A. van der Pol, and H. W. de Wijn, Phys. Rev. Lett. **37**, 1554 (1976).

[16] M. H. F. Overwijk, P. J. Rump, J. I. Dijkhuis, and H. W. de Wijn, Phys. Rev. B **44**, 4157 (1991).

[17] J. I. Dijkhuis and H. W. de Wijn, Phys. Rev. B **20**, 1844 (1979).

[18] R. J. G. Goossens, J. I. Dijkhuis, and H. W. de Wijn, Phys. Rev. B **32**, 7065 (1985).

[19] B. A. Wilson, in *Tetrahedically Bonded Amorphous Semiconductors*, edited by R. A. Street, D. K. Biegelsen, and J. C. Knights, AIP Conf. Proc. No. **73** (AIP, New York, 1981), p. 273.

[20] V. I. Kozub, A. M. Rudin, and H. R. Schober, Phys. Rev. B **50**, 6032 (1994).

[21] D. L. Williamson, A. H. Mahan, B. P. Nelson, and R. S. Crandall, Appl. Phys. Lett. **55**, 783 (1989).

[22] Y. M. Galperin, V. G. Karpov, and V. I. Kozub, Adv. Phys. **38**, 669 (1989).

[23] U. Buchenau, Y. M. Galperin, V. L. Gurevich, D. A. Parshin, M. A. Ramos, and H. R. Schober, Phys. Rev. B **46**, 2798 (1992).

[24] A. J. Scholten, Ph.D. thesis, Utrecht University, 1995, p. 111.

[25] D. A. Parshin, Phys. Rev. B **49**, 9400 (1994).

[26] N. G. Einspruch, E. J. Witterholt, and R. Truell, J. Appl. Phys. **31**, 806 (1960).

[27] L. A. Chernov, *Wave Propagation in a Random Medium* (McGraw-Hill, New York, 1960).

[28] M. P. Zaitlin and A. C. Anderson, Phys. Rev. B **12**, 4475 (1975).

[29] P. G. Klemens, Proc. Phys. Soc. A **68**, 1113 (1955).

[30] S. A. Basun, A. A. Kaplyanskiĭ, and S. P. Feofilov, Pis'ma Zh. Eksp. Teor. Fiz. **34**, 259 (1982) [JETP Lett. **34**, 246 (1981)].

[31] This assumption is, in fact, inherent to the fracton model, because even a narrow distribution of hopping distances leads to an exponentially broad distribution of hopping times (Ref. 4).

[32] R. A. Street, Adv. Phys. **30**, 593 (1981).